Spatially clustered neuronal assemblies comprise the microstructure of synchrony in chronically epileptic networks

Sarah Feldt Muldoon, Ivan Soltesz, Rosa Cossart

▶ **To cite this version:**

Sarah Feldt Muldoon, Ivan Soltesz, Rosa Cossart. Spatially clustered neuronal assemblies comprise the microstructure of synchrony in chronically epileptic networks. Proceedings of the National Academy of Sciences of the United States of America, 2013, 110 (9), pp.3567-3572. 10.1073/pnas.1216958110 . hal-01848184

HAL Id: hal-01848184
https://amu.hal.science/hal-01848184v1

Submitted on 24 Jul 2018

HAL is a multi-disciplinary open access archive for the deposit and dissemination of scientific research documents, whether they are published or not. The documents may come from teaching and research institutions in France or abroad, or from public or private research centers.

L'archive ouverte pluridisciplinaire **HAL**, est destinée au dépôt et à la diffusion de documents scientifiques de niveau recherche, publiés ou non, émanant des établissements d'enseignement et de recherche français ou étrangers, des laboratoires publics ou privés.

Spatially clustered neuronal assemblies comprise the microstructure of synchrony in chronically epileptic networks

Sarah Feldt Muldoon[a,b,c,d,1], Ivan Soltesz[a,2], and Rosa Cossart[b,c,d,2]

[a]Department of Anatomy and Neurobiology, University of California, Irvine, CA 92697-1280; [b]Institut National de la Santé et de la Recherche Médicale Unité 901, 13009 Marseille, France; [c]Aix-Marseille Université, Unité Mixte de Recherche S901, 13009 Marseille, France; and [d]Institut de Neurobiologie de la Méditerranée, 13009 Marseille, France

Edited by Eve Marder, Brandeis University, Waltham, MA, and approved January 11, 2013 (received for review September 30, 2012)

Epilepsy is characterized by recurrent synchronizations of neuronal activity, which are both a cardinal clinical symptom and a debilitating phenomenon. Although the temporal dynamics of epileptiform synchronizations are well described at the macroscopic level using electrophysiological approaches, less is known about how spatially distributed microcircuits contribute to these events. It is important to understand the relationship between micro and macro network activity because the various mechanisms proposed to underlie the generation of such pathological dynamics are united by the assumption that epileptic activity is recurrent and hypersynchronous across multiple scales. However, quantitative analyses of epileptiform spatial dynamics with cellular resolution have been hampered by the difficulty of simultaneously recording from multiple neurons in lesioned, adult brain tissue. We have overcome this experimental limitation and used two-photon calcium imaging in combination with a functional clustering algorithm to uncover the functional network structure of the chronically epileptic dentate gyrus in the mouse pilocarpine model of temporal lobe epilepsy. We show that, under hyperexcitable conditions, slices from the epileptic dentate gyrus display recurrent interictal-like network events with a high diversity in the activity patterns of individual neurons. Analysis reveals that multiple functional clusters of spatially localized neurons comprise epileptic networks, and that network events are composed of the coactivation of variable subsets of these clusters, which show little repetition between events. Thus, these interictal-like recurrent macroscopic events are not necessarily recurrent when viewed at the microcircuit scale and instead display a patterned but variable structure.

functional connectivity | neuronal networks

The synchronization of neuronal networks is a widely observed phenomenon and has been shown to have important implications in a variety of systems ranging from the development of healthy circuits (1, 2) to pathological conditions such as epilepsy (3, 4). Although the large-scale population level activity of these systems is often investigated, less is known about how individual neurons come together to create such synchronous network dynamics. The study of epilepsy from a networks perspective is of special interest, as epileptic networks can support both normal brain functioning and pathological activity. Multiple computational studies have linked the development of hypersynchronous neuronal activity associated with the disorder to changes in the underlying network connectivity (5–8), and many types of epilepsy display significant structural changes in the neuronal network such as cell loss and axon sprouting (9). In temporal lobe epilepsy (TLE), many of these changes take place in the dentate gyrus (DG), with a loss of hilar interneurons and mossy cells, as well as the addition of recurrent connections between granule cells through mossy fiber sprouting and alterations of cellular morphology (10–16).

Interictal spikes are a common feature of epileptic networks and can be identified as transient synchronous events in electroencephalography (EEG) or local field potential recordings in epileptic tissue (17). Although at the large scale, these events might seem to reflect synchronous population firing, recent studies of single-cell activity during interictal events in the human cortex suggest a wide heterogeneity in neuronal firing with different populations of neurons participating in sequential bursts (18). Additionally, the propagation of interictal spikes shows a wide spatial variance both at the large scale in EEG data from humans as well as at smaller cellular scales in rat hippocampal slice cultures (19). This suggests that the specific spatiotemporal properties of local neuronal populations play an important role in epileptic activity. Thus, to understand and better treat epilepsy, we must first determine how individual cells give rise to network dynamics, and how these dynamics relate to the structure of the underlying network.

In this study, we address the basic question of how network structure and dynamics are modified in epileptic networks by studying functional network structure at the level of single-cell resolution using multibeam two-photon calcium imaging in slices from the DG of pilocarpine-treated, chronically epileptic mice. As expected, we find that epileptic networks are more active and display large-scale synchronous neuronal activity. However, we also observe a great heterogeneity in neuronal dynamics and determine that epileptic networks exhibit a functional network structure composed of spatially localized cell clusters. Interestingly, it is the coactivation of subsets of these clusters that comprise the large scale network events, and the composition of these events continuously varies as different clusters participate in each event. We conclude that the microstructure of synchrony in epileptic networks is not as stereotyped as its large-scale expression, likely reflecting the fine underlying anatomical changes associated with epileptogenesis.

Results

To observe single-cell dynamics of both healthy and epileptic networks, we used multibeam two-photon calcium imaging of the DG in hippocampal slices obtained from either an age-matched control group (n = 19 slices, 11 mice) or an epileptic group (n = 24 slices, 9 mice) in which mice had been subjected to the pilocarpine model of TLE (*SI Materials and Methods*). A chronic model of epilepsy was used because it displays structural reorganization. In the mouse pilocarpine model of TLE, the development of spontaneous seizures has been associated with

Author contributions: S.F.M., I.S., and R.C. designed research; S.F.M. performed research; S.F.M. analyzed data; and S.F.M., I.S., and R.C. wrote the paper.

The authors declare no conflict of interest.

This article is a PNAS Direct Submission.

Freely available online through the PNAS open access option.

[1]To whom correspondence should be addressed. E-mail: sarah.muldoon@inserm.fr.

[2]I.S. and R.C. contributed equally to this work.

This article contains supporting information online at www.pnas.org/lookup/suppl/doi:10.1073/pnas.1216958110/-/DCSupplemental.

several structural network changes including cell death, axonal sprouting, increased neurogenesis, and changes in cellular morphology (20–22). Thus, by observing single-cell dynamics from a large neuronal population, the functional network organization could be described, and differences between control and epileptic groups could be related to differences in the underlying networks.

Calcium Imaging of Chronically Epileptic Tissue. Previously, calcium imaging of acute slices had largely been limited to studies of developing or juvenile tissue due to the difficulty of bulk loading adult cells with the AM-ester form of calcium dyes (23). However, the use of the pilocarpine model to generate the epileptic networks analyzed in this study required that all imaging be done on slices from adult animals whose epilepsy had been verified with telemetric EEG (*SI Materials and Methods*). We therefore developed a protocol that allowed for the bulk loading of neurons in the DG of acute slices from adult mice with the calcium dye fura-2 AM (*SI Materials and Methods*) (Fig. S1). Because under normal in vitro conditions the DG is a relatively silent structure, partly due to the rather hyperpolarized values of the resting membrane potential of granule cells (24), neuronal activity was induced through continuous perfusion of an artificial cerebrospinal fluid (ACSF) with an elevated K^+ concentration (7.5 mM) that depolarizes cells to a level comparable with the in vivo condition (25). Although others have used elevated extracellular K^+ conditions as an acute model to study epileptiform dynamics in other hippocampal regions in control slices, we simply used this protocol as a tool to induce enough activity in individual cells to calculate functional connectivity in both control and chronically epileptic networks. Upon the introduction of 7.5 mM K^+ ACSF, we observed an increase in neuronal activity, and slices were allowed to stabilize for at least 3 min before the recordings used for analysis began. Cell contours and onset times of calcium activity were identified using custom software (*SI Materials and Methods*) as previously described (26). A high level of heterogeneity was observed in the activity of cells (Fig. S1), and this diversity was seen in both control and epileptic slices.

Epileptic Networks Are More Active and Display More Network Events. When recording from slices from both control and epileptic groups, we detected the same number of cells on average (Fig. S1; 99 ± 6 cells, $n = 19$ slices, 11 control mice; 101 ± 9 cells, $n = 24$ slices, 9 epileptic mice; two-sample t test, $P = 0.0019$). However, a larger percentage of cells were active (i.e., displayed spontaneous calcium transients seen as downward deflections in Fig. S1*B*) in the epileptic group: 59 ± 2% vs. 48 ± 3% in the control group (two-sample t test, $P = 0.002$; $n = 19$ slices, 11 control mice; $n = 24$ slices, 9 epileptic mice). In addition, cells in the epileptic group had a higher activation frequency (Fig. S1 *F* and *G*; median: 4.3 onsets/min, $n = 912$ cells, 19 slices, 11 control mice; median: 6.0 onsets/min, $n = 1413$ cells, 24 slices, 9 epileptic mice; two-sample Kolmogorov–Smirnov test, $P = 0.0003$). Thus, neurons in the epileptic DG are more likely to be active and display higher activation frequencies than those in control slices. These results are consistent with the fact that epileptic networks have a higher excitability (27, 28).

We also observed (especially in epileptic slices) the presence of statistically significant synchronous network-level activity, which we refer to as network events. Similar spontaneous activity has been previously described in the DG of slices from kainate-treated rats when perfused with elevated K^+ (29). To automatically detect the presence of these large-scale events, we used a sliding window technique based on the statistical significance of the total number of calcium activations summed over all neurons within each 500-ms window (*SI Materials and Methods*) (Fig. 1*A*).

Although network events were observed in both control and epileptic slices, the frequency of events was significantly higher in epileptic slices (Fig. 1*B*; 1.9 ± 0.5 events/min, $n = 19$ slices, 11 control mice; 3.9 ± 0.8 events/min, $n = 24$ slices, 9 epileptic mice; two-sample t test, $P = 0.04$). Because not all slices displayed network events, we further divided the data into two groups: slices that displayed network events, and those that did not. Only slices that displayed more than one event per minute on average were classified as displaying network events (this allowed for further statistical analysis of network events as it meant that a typical 4-min movie contained a minimum of five events). Forty-seven percent ($n = 9$ of 19) of control slices were classified as displaying network events, whereas 71% ($n = 17$ of 24) of epileptic slices displayed events (Fig. 1*C*).

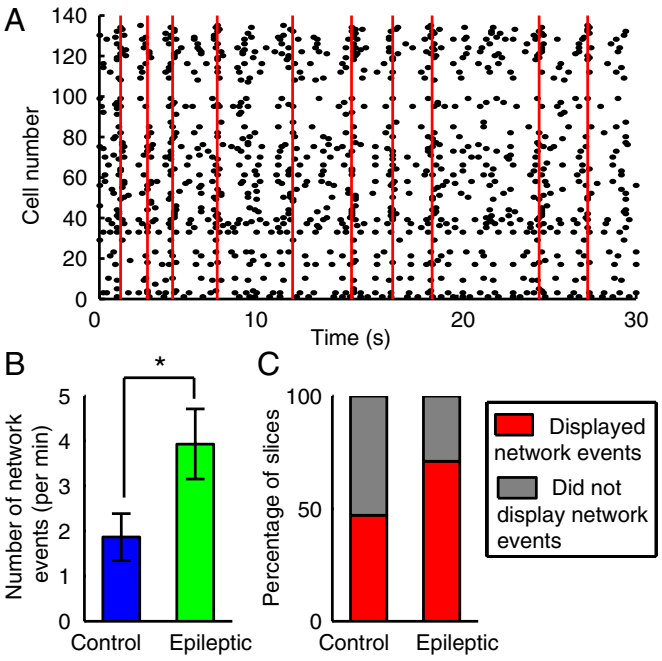

Fig. 1. Slices display network events. (*A*) Raster plot of the population dynamics after onset detection in an epileptic slice. (*B*) The frequency of network events is higher in epileptic slices ($n = 19$ slices, control; $n = 24$ slices, epileptic; two-sample t test, $P = 0.04$; error bars represent SEM). (*C*) Classification of slices that displayed network events. A slice was deemed to display network events if the frequency of detected events was greater than one event per minute.

Network Dynamics Are Composed of Synchronous Cell Clusters. We next quantified the percentage of significantly correlated pairs of neurons in each slice that displayed network events (*SI Materials and Methods*) (Fig. S2*A*). Although there was a broad range in the distribution of values, many slices in both groups contained a high percentage of significantly correlated pairs of neurons, as one might expect because we observed network events. However, the data also contained a high percentage of background activity, i.e., a large percentage of calcium onsets occurred outside of network events (Fig. S2*B*). Surprisingly, the distributions of correlations between individual neurons and network events were skewed toward low values in both control and epileptic conditions (*SI Materials and Methods*) (Fig. S2*C*; $n = 481$ cells, 9 slices, 7 control mice; $n = 1017$ cells, 17 slices, 7 epileptic mice). Thus, although the data displayed high correlations between pairs of neurons, the individual neurons did not seem to be correlated with the activity of the network as a whole, indicating that the prevalence of network events was not the only reason for the high number of pairs of significantly correlated neurons.

As the lack of high correlation between neuronal activity and network events was rather unexpected, we further examined the structure of correlations and searched for relationships within

groups of neurons. We applied the functional clustering algorithm (FCA), which was designed to detect groups of synchronous neurons in spike train data based on statistically significant similarities between firing patterns (30). This algorithm is a form of hierarchical clustering that sequentially joins neurons to create groups based on a chosen similarity metric (*SI Materials and Methods*). For each imaged network, a dendrogram representing the order of grouping was obtained (Fig. 2*A*), and the point at which the grouping was no longer statistically significant was calculated (dashed horizontal line in Fig. 2*A*). The detected groups correspond to the neurons that have been joined below this statistical threshold line and are depicted with a common color in Fig. 2. All neurons that were not joined with another neuron to form a group are depicted in gray. We defined a functional cluster to be a group consisting of three or more neurons (12 functional clusters in Fig. 2).

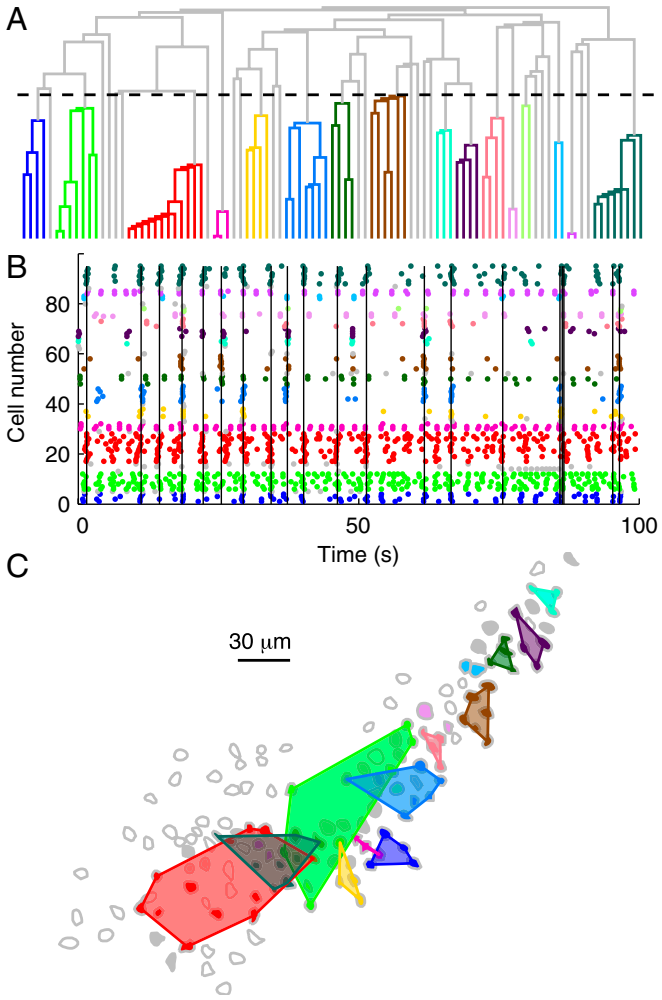

Fig. 2. Functional clustering of neuronal dynamics. (*A*) Dendrogram representing the application of the FCA to neuronal dynamics observed in an epileptic slice. The vertical axis represents the step in the algorithm, and the dashed line indicates the cutoff for statistical significance. The resulting clusters of neurons are indicated by a common color, which is held constant in all resulting plots. (*B*) Raster plot of population activity plotted with the neuron order given from the above dendrogram. Note that neurons within the same cluster do indeed display similar synchronous dynamics. The vertical black lines indicate detected network events. (*C*) Spatial mapping of the clusters of neurons depicted in *A* and *B*. A corresponding polygon enclosing the cluster has been additionally overlaid to aide in the visualization of the identified clusters. Clusters of neurons are spatially localized and arranged radially throughout the granule cell layer.

Next, we constructed raster plots of activity as a function of time, where neurons are ordered according to the functional cluster to which they belong (Fig. 2*B*). Inspection of these raster plots clearly indicates that the algorithm has grouped neurons with similar temporal dynamics. The spatial distribution of these functional clusters onto the imaged contour plots was then analyzed. In the case of epileptic networks, as quantified below, we observed that the functional clusters tended to be composed of spatially local neurons and distributed along the granule cell layer (GCL) (Fig. 2*C*).

Clusters were detected in slices from both control and epileptic groups, but epileptic slices contained more functional clusters than control slices (Fig. S3*A*; 1.6 ± 0.3 clusters/slice, $n = 19$ slices, 11 control mice; 3.0 ± 0.5 clusters/slice, $n = 24$ slices, 9 epileptic mice; two-sample t test, $P = 0.04$). There was no statistical difference between the distributions of the number of neurons comprising a cluster between the groups (two-sample Kolmogorov–Smirnov test, $P = 0.8$, $n = 30$ clusters, 15 slices, 10 control mice; $n = 72$ clusters, 22 slices, 9 epileptic mice) with the majority of clusters being composed of 3–6 neurons (Fig. S3*B*).

Epileptic Cell Clusters Are Spatially Localized. Although the number of neurons composing a cluster was similarly distributed for control and epileptic groups, marked differences were observed when clusters were spatially mapped. We first examined the spatial extent of the clusters (*SI Materials and Methods*). This metric is an inverse measure of density that quantifies the area of the cluster, normalized by the number of neurons in the cluster. Clusters with a small spatial extent will be spatially localized, whereas those with larger values will be composed of neurons spread throughout the GCL. The spatial extents of clusters from the epileptic group are highly skewed toward low values and significantly smaller than those from the control group (median: 383 μm^2/neuron, $n = 30$ clusters, 15 slices, 10 control mice; median: 151 μm^2/neuron, $n = 72$ clusters, 22 slices, 9 epileptic mice; two-sample Kolmogorov–Smirnov test, $P = 0.03$). This result is in agreement with the average pairwise distance between neurons within a cluster (Fig. 3 *A* and *B*). Again, this distribution is skewed toward low values for the epileptic group and is significantly smaller than that of the control group (median: 76 μm, $n = 30$ clusters, 15 slices, 10 control mice; median: 43 μm, $n = 72$ clusters, 22 slices, 9 epileptic mice; two-sample Kolmogorov–Smirnoff test, $P = 0.03$). Thus, clusters in epileptic slices are more spatially localized, whereas clusters in control slices tend to be composed of neurons distributed across the GCL.

The maximum distance between neurons within a cluster also showed differences between groups. In the case of the control group, the distribution was bimodal and could be fit by the sum of two Gaussians ($R^2 = 0.62$, $\chi^2 = 0.0013$, peak1 = 58 ± 8 μm, peak2 = 225 ± 11 μm), with the second mode occurring for clusters with a maximum distance >150 μm (Fig. 3*C*; $n = 30$ clusters, 15 slices, 10 control mice; $n = 72$ clusters, 22 slices, 9 epileptic mice). Thus, to investigate the differences between clusters belonging to each peak of the bimodal distribution, we further divided clusters in both control and epileptic groups into subgroups with a maximum pairwise distance of either <150 or >150 μm. For the control group ($n = 15$ slices), 53% of the detected clusters had a maximum pairwise distance of >150 μm, whereas 35% of the clusters in the epileptic group had a maximum pairwise distance of >150 μm ($n = 22$ slices). Because we were imaging the GCL, the dimensions (radial vs. tangential) of the imaging were not equal, and the radial width of the GCL was generally <150 μm. Thus, clusters with a maximum distance >150 μm were composed of neurons distributed throughout the imaging area and span the tangential axis of the GCL. Importantly, clusters distributed throughout the GCL also tended to be

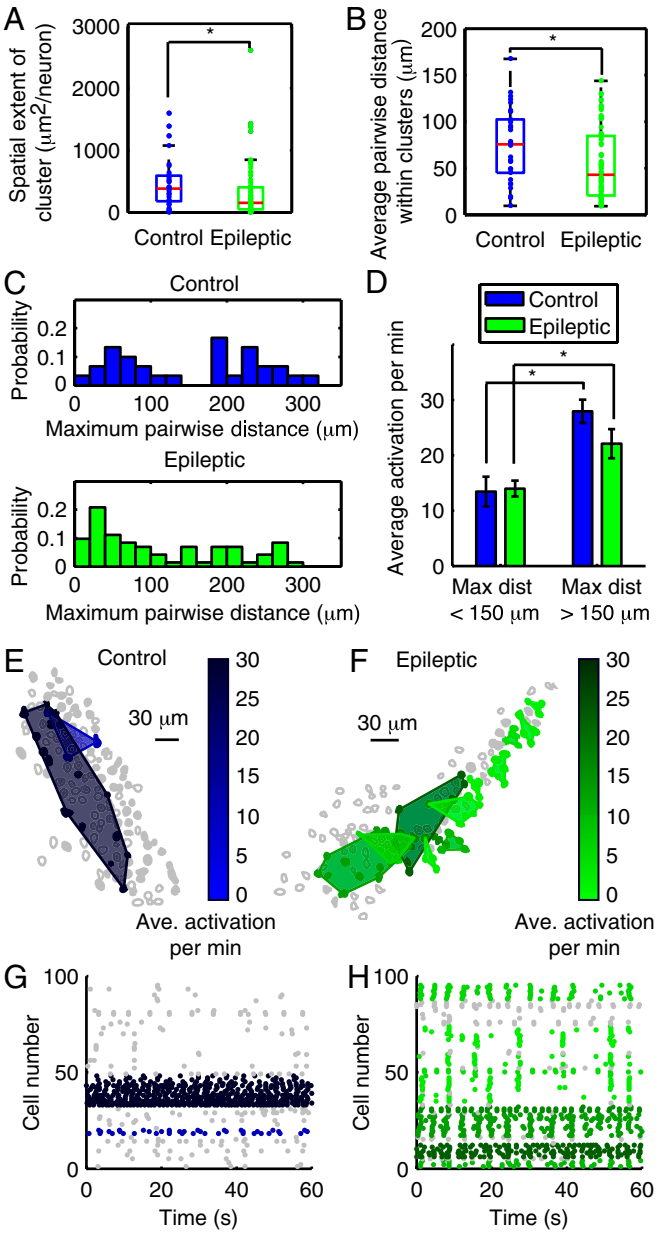

Fig. 3. Characterization of spatial properties of neuronal clusters. (*A*) Distributions of the spatial extent of control (n = 30) and epileptic (n = 72) clusters. The red lines indicate median values, and the box encloses the 25th to 75th percentiles. The distribution of clusters in epileptic tissue is highly skewed toward small values, indicating that these clusters are more spatially localized (Kolmogorov–Smirnov test, P = 0.03). (*B*) Distributions of the average pairwise distance between neurons within a cluster. Again, the distribution for epileptic tissue is skewed toward low values, confirming that these clusters tend to be spatially localized. (*C*) Probability distributions of the maximum pairwise distance within a cluster for control (*Upper*) and epileptic (*Lower*) tissue. Note the bimodal nature of the distribution in the case of clusters from control tissue. Clusters with a maximum distance of >150 μm are distributed throughout the GCL. (*D*) Average frequency of calcium activations for neurons within a cluster, separated by clusters with a maximum pairwise distance of >150 or <150 μm. Clusters with a tangential orientation (>150 μm) are composed of neurons with higher firing rates (two-sample t test; n = 14 clusters <150, n = 16 clusters >150, P = 0.00018, control; n = 25 clusters <150, n = 47 clusters >150, P = 0.004, epileptic). (*E* and *F*) Examples of the spatial mapping of clusters from a control slice (*E*) and an epileptic slice (*F*). The shade of the cluster indicates the average frequency of calcium activation for neurons within the cluster. The darker shades indicate clusters with more activity. (*G* and *H*) Raster plots depicting the activity of neurons in the clusters from *E* and *F*.

composed of tonically active neurons and were grouped together based on their high-level activity as opposed to their specific temporal patterning. Clusters with a distributed spatial layout (maximum pairwise distance of >150 μm) have a significantly higher average activation rate in both control and epileptic slices (Fig. 3*D*; two-sample t test; n = 14 clusters, 8 slices, 6 mice, maximum pairwise distance of <150 μm, control; n = 16 clusters, 13 slices, 9 mice, maximum pairwise distance of >150 μm, control, P = 0.00018; n = 25 clusters, 18 slices, 9 mice, maximum pairwise distance of <150 μm, epileptic; n = 47 clusters, 16 slices, 7 mice, maximum pairwise distance of >150 μm, epileptic, P = 0.004; differences within subgroups are not significant).

Examples of the spatial distribution and relationship to the amount of activity displayed by the cluster can be seen in Fig. 3 *E–H*. In epileptic slices, clusters are spatially localized and their raster plots show clear temporal patterning. However, in control slices, the clusters occupy a larger spatial area and are composed of highly active neurons whose continuous activity occurs independently of the network events. Thus, these continuously active clusters are unlikely to shape the overall temporal structure of network dynamics, and the observed network events are more likely to be related to the activity of the smaller, spatially localized clusters that are more frequently observed in epileptic slices.

Network Events Are Composed of the Coactivation of Different Subsets of Cell Clusters. We next explored the relationship between cluster and network dynamics by analyzing the dynamics of cluster activation (*SI Materials and Methods*). A cluster was considered active if greater than one-half of its neurons had at least one calcium onset within a 500-ms window (consistent with the window size used to detect network events; Fig. 4*A*). Although cluster–network correlations were higher on average than neuron–network correlations, many clusters still had low cluster–network correlations and there was a relatively high amount of background activity (Fig. S4 *A* and *B*), indicating that clusters were active both during and outside of network events. Additionally, the percentage of neurons that participated in each network event was highly variable and broadly distributed (Fig. S4*C*). This was consistent with the observation that many clusters were often inactive during individual network events.

We examined the structure of the network events in terms of the clusters that were activated in each event by creating a "pattern" describing the composition of each event. Each pattern was a series of 0 and 1, with each character representing a cluster. The value was 0 if the cluster was not active during the event, and 1 if the cluster was active (see Fig. 4*B* for the first eight network events depicted in Fig. 4*A*). By comparing the patterns for each event, we found that there was very little repetition of patterns meaning that, in general, each network event was composed of the coactivation of a different subset of clusters. For example, the eight events illustrated in Fig. 4*B* are all represented by unique patterns. In both the control and epileptic groups, patterns were unlikely to dominate the composition of network events, as seen in the distributions of Fig. 4*C*, which are skewed toward low values (n = 23 patterns, 3 control slices; n = 123 patterns, 10 epileptic slices). Thus, although network events appear to be similar when observed at a large global scale, analysis of the smaller scale structure of cluster and neuron participation reveals that each event is different and composed of a varying subset of coactive functional clusters.

Discussion

In this study, we explored the functional reorganization of structurally altered, chronically epileptic networks through the application of a clustering algorithm to neuronal dynamics obtained from population-level calcium imaging. Our main finding is that large-scale recurrent network synchronizations, one of the hallmarks of epilepsy, are not actually repetitive events. Instead, when

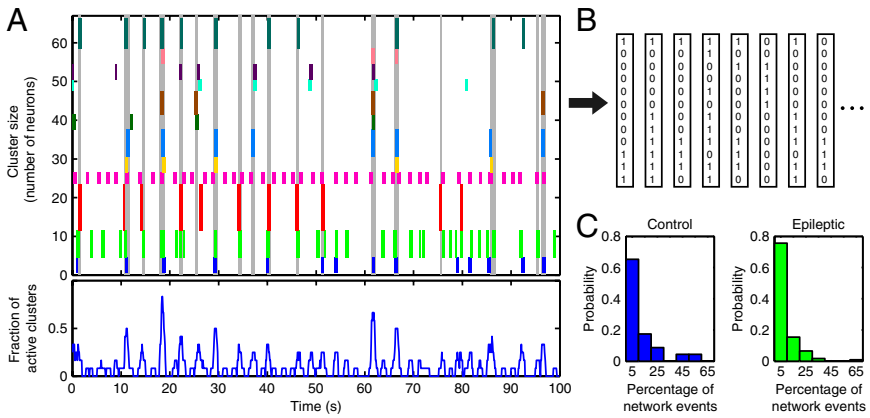

Fig. 4. Cluster activation and composition of network events. (*A*) Cluster activation raster plot (*Upper*) and corresponding fraction of active clusters as a function of time (*Lower*). The colored vertical lines depict cluster activation, and the color corresponds to the clusters identified in Fig. 2. The vertical height indicates the number of neurons comprising the cluster, and the horizontal length indicates the time window during which the cluster was active. The vertical gray lines mark detected network events, and the fraction of active clusters as a function of time is shown below. The time period shown is the same as in the raster plot from Fig. 2*B*. (*B*) Schematic depicting transformation of network events into a "pattern" of 0 and 1 in which a value of 1 indicates that the cluster was active during the network event. The vertical position of the 0/1 value in the column corresponds to the vertical position of the cluster in the raster plot. Transformation is shown for the first eight network events from *A*. (*C*) Probability distributions showing the percentage of network events that are composed of each observed pattern. Here, data are shown for patterns from slices that displayed network events and had three or more clusters ($n = 23$ patterns, 3 slices, control; $n = 123$ patterns, 10 slices, epileptic). This indicates that patterns rarely repeat, and each network event is composed of the coactivation of a different subset of clusters.

observed at the level of individual neurons, they break down into unpredictable combinations of spatially localized, coherent neuronal clusters.

Although the temporal aspects of epileptiform dynamics have been thoroughly examined using electrophysiological approaches, their microcircuit level spatial aspects have remained elusive due to the technical challenges of experimentally addressing this issue with imaging approaches. Traditionally, calcium imaging has been limited to juvenile tissue because of the difficulties associated with loading adult tissue with membrane-permeable fluorescent calcium dyes (23). Thus, spatial analysis of network bursts could only be studied in healthy juvenile slices using acute drug applications or in organotypic cultures (19, 31, 32). However, these preparations are not ideal for the study of epileptic networks because they do not exhibit the spectrum of structural changes associated with epileptogenesis. Here, we overcame the experimental difficulties of imaging adult tissue by improving the slicing and loading procedure (*SI Materials and Methods*). The quality of the slice surface was the most important parameter associated with high-quality imaging in adult slices.

Previous work using similar techniques to study the functional structure of synchronous network behavior in the developing hippocampus identified early-born GABAergic hub neurons that consistently fired at the beginning of synchronous network events, and therefore could be identified as having a high degree of functional connectivity (26, 33). Although at a large scale, these synchronous events observed during development seem similar to interictal bursts observed in models of epilepsy, it has been shown that their dynamics are deterministic, showing the same repeatable patterns in the firing of neurons (26, 31). We showed that the dynamics of the synchronous interictal-like events observed in our chronic model of epilepsy display a different and variable structure. Moreover, the specific activity patterns of neurons also showed a large heterogeneity. A diversity of neuronal activity associated with synchronous pathological behavior has also recently been observed during seizures recorded from microelectrode arrays in humans with focal epilepsy (34). This raises the intriguing possibility that pathological and physiological network dynamics could be distinguished based on the stability of their spatial components and highlights the importance of understanding how individual cells work together to produce network activity.

To further understand how the heterogeneity in neuronal dynamics related to network activity, we used the FCA to extract firing motifs within groups of neurons. Specifically, we detected small clusters of cells with synchronous times of activation and showed that, in epileptic slices, these clusters were spatially localized. Functional clusters could be detected in both control and epileptic tissue, but epileptic networks were composed of twice as many clusters as control networks. These clusters could be divided into two distinct types: spatially dispersed clusters composed of continuously active neurons, and spatially localized clusters displaying patterned activation profiles. Control networks were composed of a higher fraction of dispersed clusters, whereas localized assemblies were preferentially detected in epileptic networks. These different spatial arrangements likely reflect the anatomical reorganization occurring during epileptogenesis, although future work is needed to address the relationship between the functional and anatomical structure of these clusters.

Several mechanisms can be proposed to support the observed segmentation of synchronization within the GCL, but because epileptogenesis is associated with complex network reorganization, the exact mechanism(s) remain an open question. For example, common coherent excitatory or inhibitory inputs could serve to synchronize these neuronal assemblies as has been previously proposed (32). In this case, patterned mossy fiber sprouting onto clustered groups of neurons could locally coordinate the activity (35). Alternatively, common inhibitory inputs originating from hub-like GABAergic neurons (12) could function in resetting the activation times of neuronal clusters. Another unknown parameter is the cellular composition of these clusters. Our imaging was limited to the GCL, meaning that this apparently homogeneous cell population is in fact functionally diverse. Given the significant amount of neurogenesis associated with epileptogenesis (14, 36) and the fact that newborn granule cells differentially contribute to mossy fiber and basal dendrite sprouting depending on their age at the time of status epilepticus (37), these clusters could reflect clonally related granule cells. Unfortunately, it is currently not possible to address these questions using targeted electrophysiological recordings as in refs. 26 and 33 due to the time required to run the analysis and detect neuronal clusters.

When examining the temporal properties of clusters, we found that clusters were synchronously activated both during and out-

side of network events. Not only did the clusters involved change from event to event, but there was also very little repetition for any given pattern of composition indicating a lack of similarity between events. This surprising result means that, although the events looked similar at the large network-level scale, they are actually highly variable at the level of individual neurons. Interestingly, a similar variance in synchronization dynamics has been reported recently in human EEG recordings of single neurons during interictal spikes (18). Additionally, in cultured rat slices, Sabolek et al. (19) showed that interictal like events have a variable path of propagation. They also observed a varied path of propagation at larger scales between electrodes in human EEG recordings. Our observance of synchronous functional clusters of neuronal activity is consistent with a variable path of event propagation, as the variance in subsets of clusters participating in an event necessarily implies a varied path of propagation through the network. Whether the network bursts observed here represent locally generated or propagating events remains to be determined. This would require large-scale imaging from several hippocampal regions, which is currently impossible in the adult epileptic tissue because the low signal-to-noise ratio excludes the use of low-magnification objectives, and the CA3 region of adult tissue does not load the calcium dyes. Future studies using genetically encoded calcium indicators may improve network sampling but require the development of new analytical tools.

In conclusion, the interictal-like recurrent network events occurring in epileptic slices are not actually recurrent at the microcircuit level and are instead composed of the varying coactivation of spatially localized clusters. Although the exact mechanisms that synchronize the activity of neurons in the detected clusters remain unknown, future work should address this important question through the development of improved experimental techniques and analysis. Furthering our understanding of the interplay between micro- and network-level dynamics during pathological synchronization in epilepsy will be essential in developing therapeutic strategies against this widespread disorder.

Materials and Methods

All animal use protocols were performed under the guidelines of the French National Ethic Committee for Sciences and Health report on "Ethical Principles for Animal Experimentation" in agreement with the European Community Directive 86/609/EEC. Animal experiments were performed at the Institut de Neurobiologie de la Méditerranée with approval from the Prefecture des Bouches du Rhone, Direction départementale des services vétérinaires, Service Santé, Protection Animale et Environnement under agreement number B 13-055-19. Only male mice (*GAD67-KI-GFP* or *Dlx1/2^{CreERTM};RCE:LoxP*, n = 11 control, n = 9 epileptic) were used in this study, and no differences were observed between strains. These genetically modified mice were chosen such that future studies could focus on the contribution of labeled cell populations. Mice were divided into an epileptic group subjected to the pilocarpine model of TLE or an age-matched control group. Error bars on bar plots indicate SEM, and statistical significance is evaluated using 95% confidence. In box plots, the red horizontal lines denote the median of the distribution, and the box encloses the 25th to 75th percentiles. In this case, the error bars denote the upper and lower extremes (38). For additional details concerning the methods, see *SI Materials and Methods*.

ACKNOWLEDGMENTS. This work was supported by National Institute of Neurological Disorders and Stroke Award T32NS045540 (to S.F.M.), a 2011 International Incoming Fellowships Marie Curie Fellowship (to S.F.M.), National Institutes of Health Grant NS35915 (to I.S.), European Research Council Starting Grant 242852 (to R.C.), ERA-Net Network of European Funding for Neuroscience Research: EpiNet Grant (to R.C.), and an Equipe Fondation pour la Recherche Médicale 2008 Grant (to R.C.).

1. Allène C, et al. (2008) Sequential generation of two distinct synapse-driven network patterns in developing neocortex. *J Neurosci* 28(48):12851–12863.
2. Blankenship AG, Feller MB (2010) Mechanisms underlying spontaneous patterned activity in developing neural circuits. *Nat Rev Neurosci* 11(1):18–29.
3. Penfield W, Jasper HH (1954) *Epilepsy and the Functional Anatomy of the Human Brain* (Little, Boston) 1st Ed, p 896.
4. Bragin A, Engel J, Jr., Wilson CL, Fried I, Buzsáki G (1999) High-frequency oscillations in human brain. *Hippocampus* 9(2):137–142.
5. Netoff TI, Clewley R, Arno S, Keck T, White JA (2004) Epilepsy in small-world networks. *J Neurosci* 24(37):8075–8083.
6. Percha B, Dzakpasu R, Zochowski M, Parent J (2005) Transition from local to global phase synchrony in small world neural network and its possible implications for epilepsy. *Phys Rev E Stat Nonlin Soft Matter Phys* 72(3 Pt 1):031909.
7. Dyhrfjeld-Johnsen J, et al. (2007) Topological determinants of epileptogenesis in large-scale structural and functional models of the dentate gyrus derived from experimental data. *J Neurophysiol* 97(2):1566–1587.
8. Morgan RJ, Soltesz I (2008) Nonrandom connectivity of the epileptic dentate gyrus predicts a major role for neuronal hubs in seizures. *Proc Natl Acad Sci USA* 105(16): 6179–6184.
9. Dudek FE, Sutula TP (2007) Epileptogenesis in the dentate gyrus: A critical perspective. *Prog Brain Res* 163:755–773.
10. Spigelman I, et al. (1998) Dentate granule cells form novel basal dendrites in a rat model of temporal lobe epilepsy. *Neuroscience* 86(1):109–120.
11. Walter C, Murphy BL, Pun RY, Spieles-Engemann AL, Danzer SC (2007) Pilocarpine-induced seizures cause selective time-dependent changes to adult-generated hippocampal dentate granule cells. *J Neurosci* 27(28):7541–7552.
12. Zhang W, et al. (2009) Surviving hilar somatostatin interneurons enlarge, sprout axons, and form new synapses with granule cells in a mouse model of temporal lobe epilepsy. *J Neurosci* 29(45):14247–14256.
13. Houser CR, Esclapez M (1996) Vulnerability and plasticity of the GABA system in the pilocarpine model of spontaneous recurrent seizures. *Epilepsy Res* 26(1):207–218.
14. Parent JM, Lowenstein DH (1997) Mossy fiber reorganization in the epileptic hippocampus. *Curr Opin Neurol* 10(2):103–109.
15. Ratzliff Ad, Santhakumar V, Howard A, Soltesz I (2002) Mossy cells in epilepsy: Rigor mortis or vigor mortis? *Trends Neurosci* 25(3):140–144.
16. Santhakumar V, Aradi I, Soltesz I (2005) Role of mossy fiber sprouting and mossy cell loss in hyperexcitability: A network model of the dentate gyrus incorporating cell types and axonal topography. *J Neurophysiol* 93(1):437–453.
17. Kramer MA, Cash SS (2012) Epilepsy as a disorder of cortical network organization. *Neuroscientist* 18(4):360–372.
18. Keller CJ, et al. (2010) Heterogeneous neuronal firing patterns during interictal epileptiform discharges in the human cortex. *Brain* 133(Pt 6):1668–1681.
19. Sabolek HR, et al. (2012) A candidate mechanism underlying the variance of interictal spike propagation. *J Neurosci* 32(9):3009–3021.
20. Cavalheiro EA, Santos NF, Priel MR (1996) The pilocarpine model of epilepsy in mice. *Epilepsia* 37(10):1015–1019.
21. Scorza FA, et al. (2009) The pilocarpine model of epilepsy: What have we learned? *An Acad Bras Cienc* 81(3):345–365.
22. Curia G, Longo D, Biagini G, Jones RS, Avoli M (2008) The pilocarpine model of temporal lobe epilepsy. *J Neurosci Methods* 172(2):143–157.
23. Namiki S, Sasaki T, Matsuki N, Ikegaya Y (2009) Regional difference in stainability with calcium-sensitive acetoxymethyl-ester probes in mouse brain slices. *Int J Neurosci* 119(2):214–226.
24. Pan E, Stringer JL (1997) Role of potassium and calcium in the generation of cellular bursts in the dentate gyrus. *J Neurophysiol* 77(5):2293–2299.
25. Hahn TT, Sakmann B, Mehta MR (2007) Differential responses of hippocampal subfields to cortical up-down states. *Proc Natl Acad Sci USA* 104(12):5169–5174.
26. Bonifazi P, et al. (2009) GABAergic hub neurons orchestrate synchrony in developing hippocampal networks. *Science* 326(5958):1419–1424.
27. Prince DA, Tseng GF (1993) Epileptogenesis in chronically injured cortex: In vitro studies. *J Neurophysiol* 69(4):1276–1291.
28. Zhang W, Huguenard JR, Buckmaster PS (2012) Increased excitatory synaptic input to granule cells from hilar and CA3 regions in a rat model of temporal lobe epilepsy. *J Neurosci* 32(4):1183–1196.
29. Patrylo PR, Dudek FE (1998) Physiological unmasking of new glutamatergic pathways in the dentate gyrus of hippocampal slices from kainate-induced epileptic rats. *J Neurophysiol* 79(1):418–429.
30. Feldt S, Waddell J, Hetrick VL, Berke JD, Zochowski M (2009) Functional clustering algorithm for the analysis of dynamic network data. *Phys Rev E Stat Nonlin Soft Matter Phys* 79(5 Pt 2):056104.
31. Takano H, et al. (2012) Deterministic and stochastic neuronal contributions to distinct synchronous CA3 network bursts. *J Neurosci* 32(14):4743–4754.
32. Takahashi N, Sasaki T, Matsumoto W, Matsuki N, Ikegaya Y (2010) Circuit topology for synchronizing neurons in spontaneously active networks. *Proc Natl Acad Sci USA* 107(22):10244–10249.
33. Picardo MA, et al. (2011) Pioneer GABA cells comprise a subpopulation of hub neurons in the developing hippocampus. *Neuron* 71(4):695–709.
34. Truccolo W, et al. (2011) Single-neuron dynamics in human focal epilepsy. *Nat Neurosci* 14(5):635–641.
35. Bragin A, Wilson CL, Engel J, Jr. (2000) Chronic epileptogenesis requires development of a network of pathologically interconnected neuron clusters: A hypothesis. *Epilepsia* 41(Suppl 6):S144–S152.
36. Parent JM (2007) Adult neurogenesis in the intact and epileptic dentate gyrus. *Prog Brain Res* 163:529–540.
37. Kron MM, Zhang H, Parent JM (2010) The developmental stage of dentate granule cells dictates their contribution to seizure-induced plasticity. *J Neurosci* 30(6): 2051–2059.
38. Mcgill R, Tukey JW, Larsen WA (1978) Variations of box plots. *Am Stat* 32(1):12–16.

Supporting Information

Feldt Muldoon et al. 10.1073/pnas.1216958110

SI Materials and Methods

Pilocarpine Model of Temporal Lobe Epilepsy. Mice aged postnatal day 28 (P28) to P35 were first given injections of scopolamine methyl nitrate (1 mg/kg, i.p.), followed 20–30 min later by an injection of pilocarpine (300–340 mg/kg, i.p.). Animals were continuously observed to identify the onset of status epilepticus (SE). Mice that did not enter SE within 1 h of the initial injection of pilocarpine were given an additional half dose of pilocarpine to aid in the induction of SE. Mice received diazepam (10 mg/kg, i.p.) 60–90 min after the onset of SE, and this injection was repeated as needed to help terminate seizures. Animals that did not develop SE were not used for experiments. Mice were given water-soaked food and allowed to recover for at least 1 wk after pilocarpine injections before the implantation of a telemetric EEG system (Data Sciences International), which was used to continuously monitor EEG activity. EEG transmitters were implanted under anesthesia (110 mg/kg ketamine and 6 mg/kg xylazine) with electrodes attached to screws located –1.5 mm lateral, –1.5 mm posterior relative to bregma and secured with dental cement (1). At the time of surgery, mice were injected with antibiotics and analgesics (Rimadyl, 5 mg/kg; Baytril, 5 mg/kg). Injections of analgesics were continued twice daily for 2 d following the surgery, and antibiotics were administered orally in the water. EEG activity was continuously recorded, and custom-made software (MATLAB, MathWorks) was used to analyze the signal and detect the development of spontaneous seizures. Upon the detection of at least two spontaneous seizures, the mouse was considered to be epileptic and was used for imaging studies.

Slice Preparation and Calcium Loading. Horizontal slices (400 μm) were obtained from male mice (both control and epileptic) aged 2–5 mo that were first anesthetized (110 mg/kg ketamine and 6 mg/kg xylazine) and perfused transcardially with an ice-cold modified artificial cerebrospinal fluid (mACSF) containing the following (in mM): 126 choline, 2.5 KCl, 1.25 NaH_2PO_4, 7 $MgCl_2$, 0.5 CaCl, 26 $NaHCO_3$, 5 glucose. Slices were made using a Leica VT1200 S vibratome in the same mACSF used for perfusion. After being allowed to rest for at least 1 h in a solution containing one-half mACSF and one-half ACSF (ACSF composition in mM: 126 NaCl, 2.5 KCl, 1.25 NaH_2PO_4, 2 $MgCl_2$, 2 CaCl, 26 $NaHCO_3$, 10 glucose), slices were transferred to a custom-made oxygenated loading chamber, where they were bulk loaded with a calcium dye solution (10 μM fura-2 AM, 0.0016% Pluronic F-127, 2.5 mM probenecid) in ACSF at a temperature of 32 °C for 30 min. This dye has the advantage over other commonly used calcium dyes in that it fluoresces in its unbound state and is quenched in the bound state, allowing one to easily evaluate the quality of loading, even in the absence of neuronal activity. Slices were then allowed to rest and rinse in ACSF at room temperature for at least 30 min before imaging began. During imaging, slices were perfused at a rate of 3 mL/min with continuously aerated [95% (vol/vol) O_2/5% (vol/vol) CO_2] ACSF at 35–57 °C. To induce neuronal activity, the ACSF was adjusted to an elevated KCl concentration of 7.5 mM. This protocol increases the excitability of the system and has been shown to induce the appearance of synchronous network events (2, 3).

Multibeam Two-Photon Calcium Imaging. Imaging was performed using a multibeam two-photon pulsed laser-scanning system (LaVision Biotech) coupled to a microscope as previously described (4). Images were acquired using a CCD camera at a rate of 10 Hz (4 × 4 binning; pixel size, 1.2 μm; imaging field, 300 × 300 μm) with a low-magnification, high–numerical-aperture objective (20×; N.A., 0.95; Olympus), and movies generally lasted 250 s. In general, imaging was restricted to neurons in the granule cell layer due to the fact that these cells sat in a different focal plane than other cells in the slice. Only movies in which at least 50 cells could be detected and at least 30% of cells were active when perfused with ACSF with an elevated K^+ were analyzed. Slices were allowed to acclimate to the elevated K^+ for at least 3 min before movies used in the analysis were performed.

Extraction of Cell Location and Calcium Onsets. Recorded fluorescence movies were first corrected for movement artifacts using the StackReg plug-in for ImageJ. Stable portions of movies (range of 90–250 s, one movie per slice) were then imported to MATLAB for semiautomatic cell contour detection using custom-made software (4). The calcium fluorescence signal for each detected cell was obtained (Fig. S1 *A* and *B*). In these traces, the large downward deflections indicate calcium events that correspond to the firing of action potentials by the neuron (Fig. S1*C*) and were blocked when adding 2,3-dihydroxy-6-nitro-7-sulfonyl-benzo[*f*] quinoxaline (NBQX) (10 μM), D-2-amino-5-phosphonovaleric acid (D-APV) (40 μM), gabazine (10 μM), and tetrodotoxin (TTX) (1 μM) to the perfusion saline. (The percentage of active cells was reduced to 1.1 ± 0.4% for control, $n = 4$ slices, and 8 ± 4% for epileptic, $n = 2$ slices.) The onset of each deflection was marked using custom-made software (MATLAB, ref. 5), thus converting the activity of each cell in the network into a set of calcium activation onset times. The remaining analysis was performed using the extracted calcium onset times for each detected cell, along with the spatial location of the cell, which was defined to be the centroid of the contour defining the cell.

Detection of Network Events. Network events were detected using statistical significance obtained from comparison with surrogate data sets. We used a sliding window technique to detect synchronous activation of cells in the data by counting the total number of calcium onsets within a 500-ms (five frames) window. The use of a window was necessary given the timescale of synchronous wave-like events seen in the data. The window was sequentially shifted by 100 ms (one frame) to create a time series representative of the population activity. Surrogate datasets ($n = 1{,}000$) were then created using interspike interval reshuffling, and the sliding window analysis was performed. For each surrogate set, the value of the window with the maximum number of total onsets was recorded, and the cumulative distribution function (CDF) of maximum onset counts was used to calculate the 95% significance threshold. The beginning of a network event was defined to be the point in time when the onset count first crossed above the significance threshold, and the end of a network event was defined to be the time when the onset count subsequently crossed below the significance threshold. Slices were said to display network events if the frequency of detected events was greater than one event per minute (this corresponds to more than four events in the course of an average movie).

Pairwise Neuron Correlations. Pairwise correlations between neurons were calculated using the maximum normalized cross-correlation. First, spike trains of calcium onset times were convolved with a Gaussian with a SD of one movie frame (100 ms) and the signal was demeaned. The normalized cross-correlation, $\hat{C}$, between two onset trains, s_i and s_j, was calculated as follows:

$$\hat{C}(s_i, s_j)(\tau) = \frac{C(s_i, s_j)(\tau)}{\sqrt{C(s_i, s_i)(0) \cdot C(s_j, s_j)(0)}}, \quad \text{[S1]}$$

where τ is the time lag between the two signals and C is the linear cross-correlation given by the following:

$$C(s_i, s_j)(\tau) = \int_{-\infty}^{\infty} s_i(t+\tau) s_j(t) dt. \quad \text{[S2]}$$

This calculation was done for τ between −500 and 500 ms, and the maximum value, $C_{\max}$, of these calculations was selected to be the pairwise correlation between the two neurons. For each pair of onset trains, surrogate datasets (n = 1,000) were also created through the reshuffling of onset times. The calculation of $C_{\max}$ was repeated for the surrogate datasets and the 95% significance threshold was calculated from the CDF of these values. For each slice that displayed network events, we then calculated the percentage of pairs of neurons with statistically significant values of $C_{\max}$ as presented in Fig. S2.

Neuron–Network Correlations. To calculate correlations between individual neurons and network events, neurons were represented by an array of 0 and 1, where 0 represented quiescent movie frames and 1 represented a calcium onset. Similarly, the activity of the network was represented by an array of 0 and 1, where all frames between beginning and end of a network event (calculated as described above) were set to be 1. The arrays were demeaned and the neuron–network correlation values were calculated for each slice as $\hat{C}(s_i, s_n)(0)$ using Eq. **S1**, where s_n is fixed to be the activity of the network. The calculation was done only for slices that displayed network events.

Detection of Functional Cell Clusters. To detect functional cell clusters, we used the functional clustering algorithm (FCA) (please see ref. 6 for a complete description of the algorithm). This algorithm was chosen because it groups neurons with statistically similar temporal firing patterns. Additionally, it does not require an a priori knowledge of the number of groups and instead determines the correct number of groupings based upon statistical significance, making it ideal for the detection of functional clusters of correlated neurons in our data. As in ref. 6, we used 95% significance levels and chose our pairwise similarity metric between spike trains i and j to be the average minimum distance Θ_{ij}, where

$$\Theta_{ij} = \frac{D_{ij} + D_{ji}}{2}, \quad \text{[S3]}$$

$$D_{ij} = \frac{1}{N_i} \sum_k \Delta t_k^i, \quad \text{[S4]}$$

and Δt_k^i is taken to be the distance from each spike, k, in train i to the closest spike in train j, with N_i being the total number of spikes in train i. The size of the window used for jittering to create the surrogate data used in the significance calculation of the algorithm was taken to be 4 s based on the timescale of the length of observed network events (6). Although this algorithm returns "groups" of all sizes (including groups of one or two neurons total), we only considered a group to be a functional cluster if it was comprised of three or more neurons. Importantly, due to the design of the algorithm and use of statistical significance in determining the point to cease clustering, the temporal activity of neurons within a given group is statistically similar, but activity patterns between groups are statistically different.

Spatial Properties of Cell Clusters. To analyze the spatial properties of clusters detected using the FCA, each cell's spatial location was defined to be the centroid of the contour used to define the cell. The spatial extent of each cluster was then defined to be the area of the polygon defining the cluster's convex hull, which was then normalized by dividing by the total number of cells comprising the cluster. The convex hull is defined as the minimal convex set containing all of the points in the cluster and can be thought of, informally, as the polygon created by connecting the points that define the perimeter of the cluster. Thus, the spatial extent represents a form of inverse density. Pairwise distances between cells were calculated using standard Euclidian distances calculated from cell centroids.

Activation of Clusters. To detect the activation of clusters, we used a sliding window technique with a window size of 500 ms (the same size as used to detect network events). A cluster was defined to be active during a given window if >50% of the cells had at least one calcium onset within the window.

Cluster–Network Correlations. To calculate correlations between cluster activation and network events, cluster activity was represented by an array of 0 and 1, where 0 represented quiescent movie frames and 1 represented all frames during which the cluster was active (see previous section). As in the case of the neuron–network correlations, the activity of the network was represented by an array of 0 and 1, where all frames between beginning and end of a network event were set to be 1. The arrays were demeaned and the cluster–network correlation values were calculated for each slice as $\hat{C}(s_i, s_n)(0)$ using Eq. **S1**, where s_n is fixed to be the activity of the network, and i is indexed across all clusters within a slice. The calculation was done only for slices that displayed network events.

1. Pitsch J, et al. (2007) Functional role of mGluR1 and mGluR4 in pilocarpine-induced temporal lobe epilepsy. *Neurobiol Dis* 26(3):623–633.
2. Rutecki PA, Lebeda FJ, Johnston D (1985) Epileptiform activity induced by changes in extracellular potassium in hippocampus. *J Neurophysiol* 54(5):1363–1374.
3. Patrylo PR, Dudek FE (1998) Physiological unmasking of new glutamatergic pathways in the dentate gyrus of hippocampal slices from kainate-induced epileptic rats. *J Neurophysiol* 79(1):418–429.
4. Crépel V, et al. (2007) A parturition-associated nonsynaptic coherent activity pattern in the developing hippocampus. *Neuron* 54(1):105–120.
5. Bonifazi P, et al. (2009) GABAergic hub neurons orchestrate synchrony in developing hippocampal networks. *Science* 326(5958):1419–1424.
6. Feldt S, Waddell J, Hetrick VL, Berke JD, Zochowski M (2009) Functional clustering algorithm for the analysis of dynamic network data. *Phys Rev E Stat Nonlin Soft Matter Phys* 79(5 Pt 2):056104.

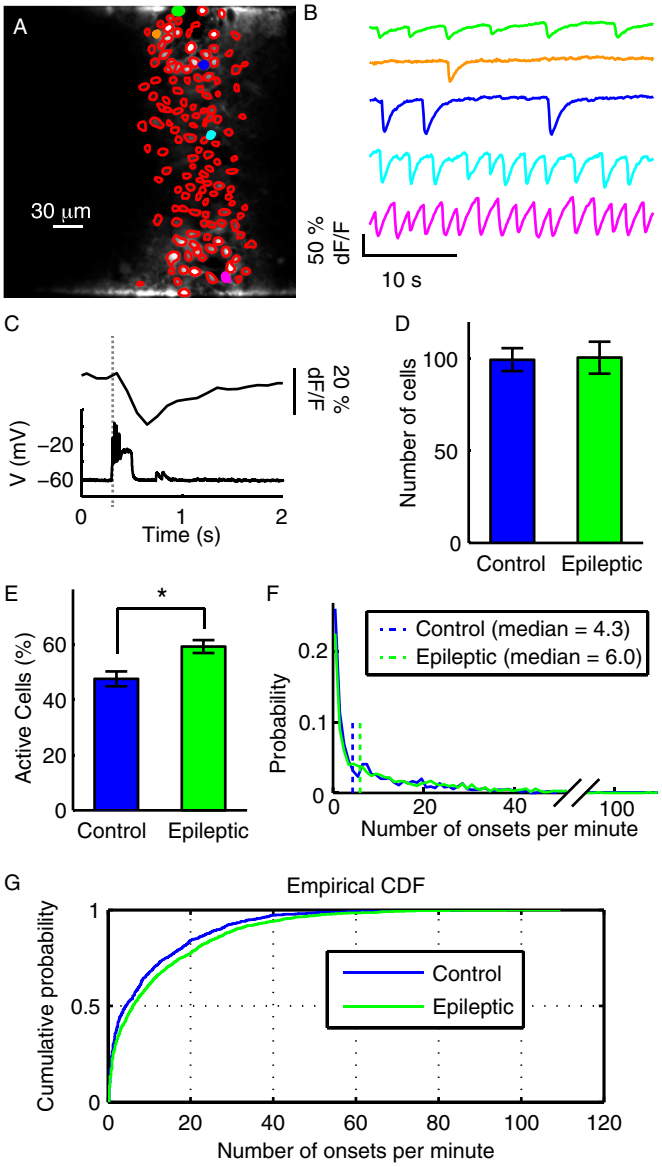

Fig. S1. Population calcium imaging of neuronal dynamics in control and epileptic tissue. (*A*) Fluorescence image of granule cell layer neurons in the DG of an acute slice from a 2-mo-old pilocarpine-treated mouse loaded with fura-2 AM. Contours of detected cells are displayed in red. (*B*) Traces showing 30 s of calcium dynamics from the five neurons with corresponding color-filled contours in *A*. Recording was done in the presence of 7.5 mM K^+ ACSF. Downward deflections in the calcium signal correspond to the firing of action potentials by the neuron and are referred to as a calcium activation onset. (*C*) Calcium fluorescence signal (upper trace) and membrane potential (lower trace) for a cell held at resting potential under current-clamp conditions. There is a clear correspondence between the firing of action potentials by the neuron and a downward deflection in the calcium signal. (*D*) Average number of cells detected and analyzed in movies from both control ($n = 19$) and epileptic ($n = 24$) tissue. Error bars represent SEM. (*E*) Average percentage of active cells in slices. A higher percentage of cells are active in epileptic slices (two-sample t test, $P = 0.0019$). (*F*) Probability distribution function indicating that neurons from both control and epileptic tissue display a heavy-tailed distribution of onset rates. (*G*) CDF comparison of the distributions in *F*. Although the distributions look similar, cells from epileptic tissue have a statistically smaller CDF (two-sample Kolmogorov–Smirnov test, $P = 0.0003$) meaning that cells in epileptic tissue tend to have a higher frequency of activation.

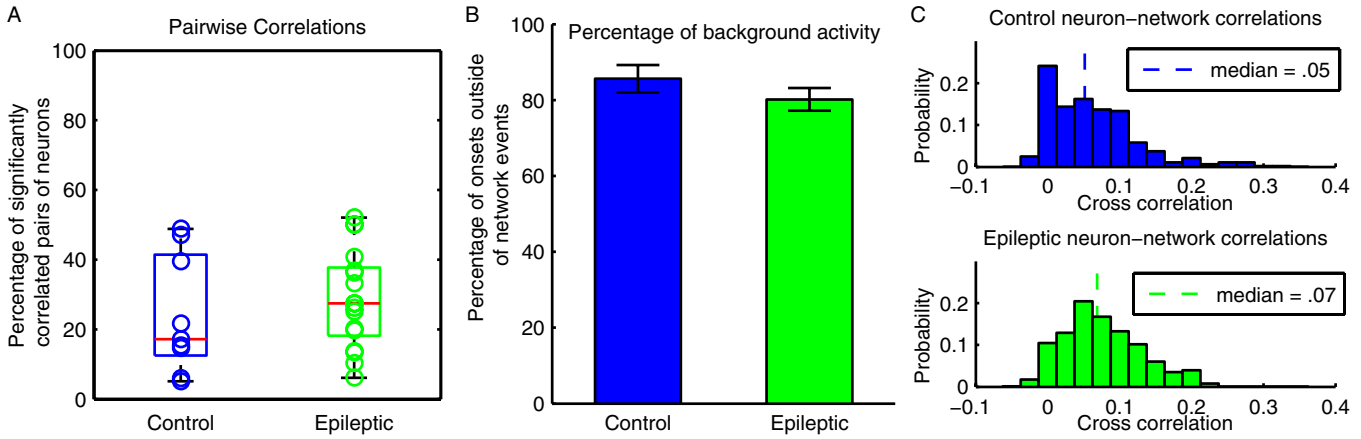

Fig. S2. Neuron–neuron and neuron–network correlations in slices which displayed network events. (*A*) Percentage of significantly correlated pairs of neurons based on comparison of maximum normalized cross-correlations to that from surrogate data for slices from control ($n = 9$) and epileptic ($n = 17$) tissue. The red lines indicate median values (median: 17.2%, control; median: 27.4%, epileptic), and the box encloses the 25th to 75th percentiles. Both distributions span a wide range of values and many slices have a high percentage of statistically correlated pairs of neurons. (*B*) Average percentage of calcium onsets that occur outside of network events. Error bars indicate SEM. In both control and epileptic slices, there is a high amount of activity that occurs between network events. (*C*) Probability distributions of the cross-correlation between a single neuron and network events for slices from control (*Upper*) and epileptic (*Lower*) tissue. In both cases, the distribution is skewed toward low values.

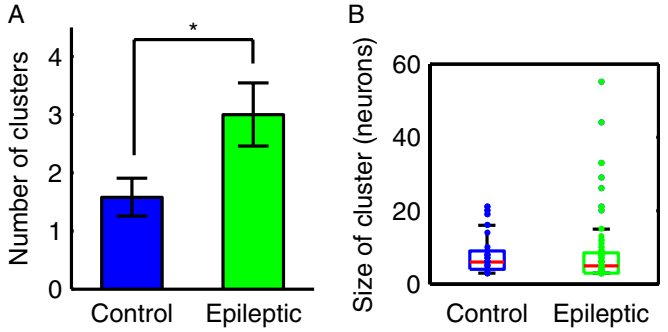

Fig. S3. Spatially distributed clusters are composed of highly active neurons. (*A*) Average number of identified clusters from application of the FCA to population dynamics from control ($n = 19$) and epileptic ($n = 24$) slices. Epileptic tissue was composed of a higher number of clusters on average (two-sample t test, $P = 0.04$). (*B*) Distributions of the number of neurons comprising each cluster. The red lines indicate median values, and the box encloses the 25th to 75th percentiles. The distributions are not statistically different (Kolmogorov–Smirnov test, $P = 0.8$), and both are skewed toward small values.

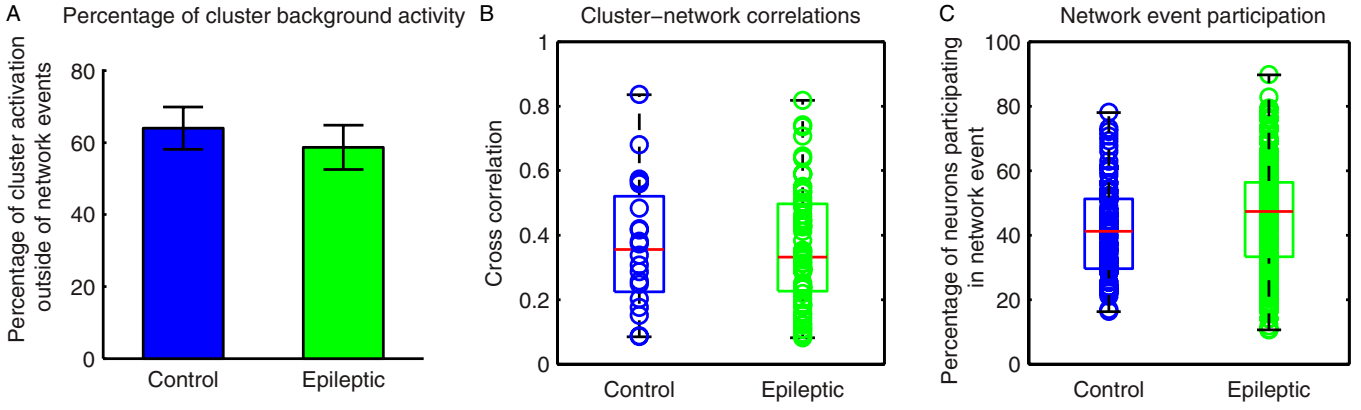

Fig. S4. Cluster–network correlations and neuron event participation in slices that displayed network events. (*A*) Average percentage of cluster activation onsets that occur outside of network events. Error bars indicate SEM. In both control ($n = 9$) and epileptic ($n = 17$) slices, clusters are often active outside of network events. (*B*) Probability distributions of the cross-correlation between a single cluster and network events. The red lines indicate median values, and the box encloses the 25th to 75th percentiles. Although some clusters are highly correlated with network events, both distributions span a large range and many clusters are lowly correlated with the network. (*C*) Distribution of the percentage of active neurons that participate in a given network event. The number of neurons that participate in each event is highly variable, indicating a lack of similarity between events.